Stress partition on the Palu-Koro fault controlling the 2018 Mw 7.5 Palu earthquake and its seismic hazards

Chang Liu [1]* and Yaolin Shi[2]

1 State Key Laboratory of Marine Geology, Tongji University, Shanghai, China

2 Key Laboratory of Computational Geodynamics, Chinese Academy of Sciences, Beijing, China

* Corresponding author: Chang Liu (changliuu@tongji.edu.cn)

Highlight:

The 1996 earthquake (Mw = 7.9) on the Minahassa thrust triggered the 2018 Palu earthquake.

The stress shadows in the Palu-Koro fault controlled the 2018 Palu earthquake rupture's southward unilateral propagation and termination.

Stress promotions in the two seismic gaps to the north and south ends of the Palu-Koro fault have increased the future seismic and tsunami hazards.

Abstract: The Mw 7.5 Palu earthquake struck the Palu-Koro fault on September 28, 2018 in the Sulawesi Island, Indonesia. Previous studies suggested that the predominantly unilateral southward rupture of this earthquake unzipped the central part of the Palu-Koro fault. Two seismic gaps were left to the north and south ends of the Palu-Koro fault. To date, the cause for earthquake generation has yet to be investigated. As a result, the reasons behind the earthquake rupture's southward unilateral propagation and termination remain unclear. The hazards of the two seismic gaps at the north and south ends of the Palu-Koro fault have yet to be explored. As such, the present study calculated the Coulomb stress change that was induced by historical large earthquakes within the target region. The stress partition and evolution on the Palu-Koro fault were examined before and after the 2018 Palu earthquake. We found that the 1996 earthquake (Mw = 7.9) on the Minahassa thrust triggered the 2018 Palu earthquake by promoting stress at the epicenter of the 2018 earthquake. The stress shadow close to the north of the epicenter of the earthquake acted as a stress barrier by preventing the earthquake northward rupture. However, the southward earthquake propagation was terminated by the stress shadow to the south of the rupture. These stress shadows were caused by the historical earthquakes on the Palu-Koro fault. Stress promotions in the two seismic gaps of the Palu-Koro fault produced by 2018 Palu earthquake have resulted in increased seismic and tsunami hazards, calling close attention to hazard prevention in central Sulawesi. Our results are important for understanding the stress migration and the induced seismic activity in the thrust and strike-slip faults system globally.

Keywords: 2018 Palu earthquake; Unilateral rupture; Rupture termination; Stress trigger; the Palu-Koro fault; Stress shadow

1. Introduction

The Mw 7.5 Palu earthquake struck the Palu-Koro fault on September 28, 2018 in the Sulawesi Island, Indonesia (Figure 1). This earthquake caused catastrophic disaster to the region of central Sulawesi by claiming over 2,000 lives, affecting more than 53,000 people, and destroying over 68,400 facilities (Song et al., 2018). The Palu-Koro fault was thought to have a high potential of large earthquakes, since it was quiescent during the past 100 years (Walpersd et al., 1998; Socquet et al., 2019). Although the Palu-Koro fault is highly likely to produce high-magnitude earthquakes (Stevens et al., 1999; Socquet et al., 2019), the generative mechanism of the 2018 Mw 7.5 Palu earthquake has yet to be investigated.

Following the first year of the shock, many researchers explored the earthquake rupture process through geodetic and seismic data inversion. The earthquake rupture is highly suspected to present predominantly unilateral southward propagation (Bao et al., 2019; Fang et al., 2019; Socquet et al., 2019; Song et al., 2019; Ulrich et al., 2019; Wang et al., 2019; Cevikbilen et al., 2019; USGS). The along strike rupture on the Palu-Koro fault propagated southward for about 130 km to 140 km. In comparison, northward propagation was observed for only about 20 km to 30 km (Socquet et al., 2019; Song et al., 2019). Significant attention was focused towards the 2018 Palu earthquake rupture's southward unilateral propagation and termination during the past one year. However, the main reasons remain unclear.

The Palu-Koro fault extends around 460 km N-S from the west of Minahassa trench to the north of Matano fault. The 2018 Palu earthquake only ruptured the central part (about 160 km) of the Palu-Koro fault (Bao et al., 2019; Fang et al., 2019; Socquet et al., 2019; Song et al., 2019; Ulrich et al., 2019; Wang et al., 2019; Cevikbilen et al., 2019; USGS). Two seismic gaps were left to the north offshore and the south on shore of the Palu-Koro fault with the length of about 180 km and 120 km, respectively (Figure 1). However, the occurrence of imminent seismic gap ruptures remains an open question. As such, it is essential to estimate any future seismic and tsunami hazards within and surrounding central Sulawesi.

Earthquake triggering by the Coulomb stress change (ΔCFS) has been previously suggested to significantly influence seismic activities in approximate distances (Simpson et al., 1988; Stein et al., 1994; Jaumé and Sykes, 1996; Nostro et al., 1997; Harris, 1998; McCloskey et al., 2005; Parsons et al., 2008; Liu et al., 2017, 2018). In order to investigate those questions above, the present study calculated the ΔCFS produced by eight large historical earthquakes (M > 6.0) with available focal mechanism on and around the Palu-Koro fault. We also calculated the ΔCFS due to the 2018 Palu earthquake. Stress partition on the Palu-Koro fault prior to 2018 was examined to evaluate any 2018 Palu earthquake triggers as well as their impact on the predominantly southward unilateral rupture propagation and termination. By predicting the combined stress evolution after 2018, we estimated the future hazards of the seismic gaps in the Palu-Koro fault.

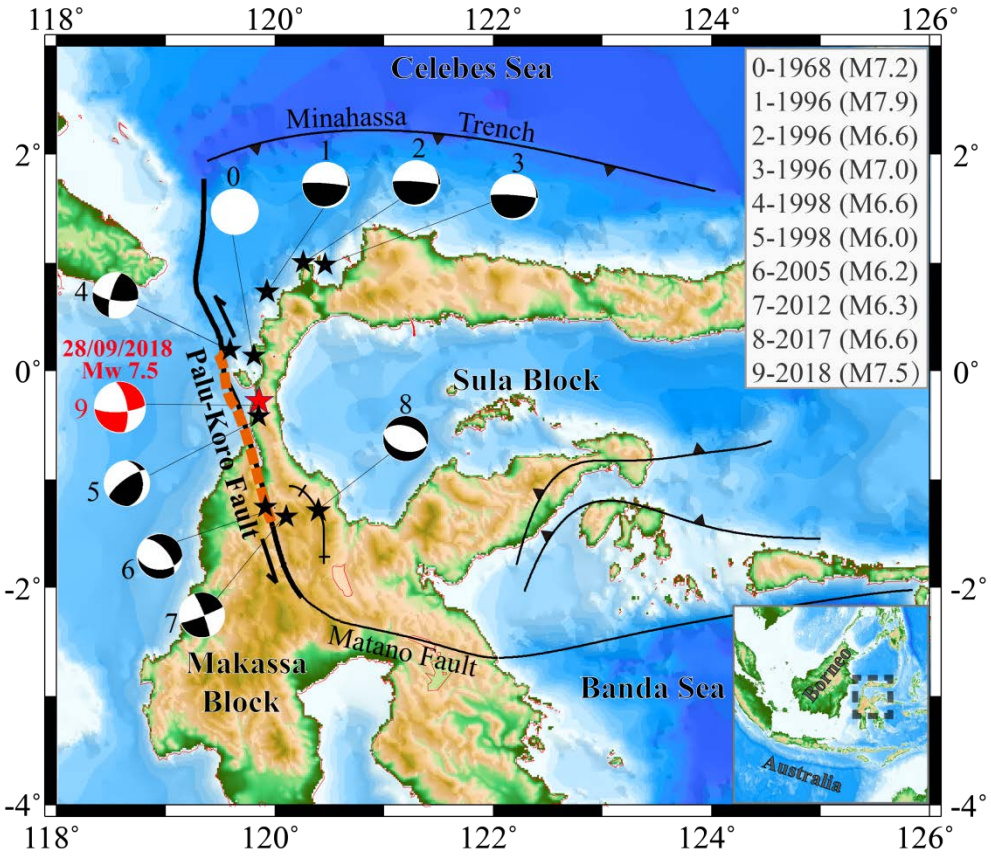

Figure 1: Tectonic setting of the Sulawesi Island, wherein the black stars define the M≥6.0 earthquakes spatial distribution on the Palu-Koro fault as well as the M≥6.5 earthquakes around the Palu-Koro fault (distance of <200 km away from 2018 Palu earthquake epicenter); the red star defines the 2018 Palu earthquake epicenter; the beach balls define the historical earthquake focal mechanism (Nos. 1-9); the white solid circle defines the 1968 earthquake unavailable focal mechanism (No. 0); and the black lines define the faults. The detailed earthquake parameters (occurrence date, focal depths, and focal mechanisms) are summarized in Table S1 (see supporting information). The red dash line presents the 2018 Palu earthquake rupture. The upper right inset shows the date and magnitude of the earthquakes (Nos. 1-9). The lower right inset presents the location of target area in the larger geological setting.

2. Geological setting

Sulawesi is located within central Southeast Asia that is prone to microplate interaction, specifically, interaction between the Indo-Australian, Philippine Sea, and Sunda plates (Hall, 1996). Sulawesi Island moves northwestward following clockwise rotation about 4°/Ma. In comparison, the Australian plate drifts northward, the Philippine Sea plate moves westward, and Sunda plate blocks the west (Vigny et al., 2002; Socquet et al., 2006). The Celebes Sea floor subducts the northern region beneath Sulawesi, and the Minahassa trench accommodates the northwestward movements of the Sula block relative to the Sunda plate (Socquet et al., 2006). The left-lateral strike-slip Palu-Koro fault, which roughly strikes the NS, is the main active structure of the western Sula block and has a high long - term slip rate of

approximately 40 mm/a. This fault connects the Minahassa subduction zone in the north with the Matano fault in the southeast, thereby running off-shore through the narrow Palu basin. Both the Palu-Koro fault and Matano fault accommodate the relative motion between the North Sula block and the Makassar block. The Palu-Koro fault has a total length of around 460 km, of which 240 km is off-shore (Watkinson and Hall, 2016). This fault is very important due to its close distance to Palu city with the population of more than 340,000. The 2018 earthquake epicenter is located approximately 75 km north of Palu city, which was heavily damaged by the earthquake triggered tsunami and landslide in some regions (Figure 1).

Sulawesi is highly seismically active. However, the Palu-Koro fault exhibits relatively low seismicity levels during the past century (Bellier et al., 2001). Records of historical seismicity in Sulawesi region are poor. Although several damaging earthquakes, such as the 1968 tsunami generating earthquake (M = 7.2), occurred along and around the Palu-Koro fault (Katili, 1970; Hamilton, 1979; Beaudouin, 1998), the details of these historical earthquakes are rarely known. Only eight large historical earthquakes (M>6.0) since 1968 were recorded and provided with focal mechanism within a distance of <200 km away from the 2018 Palu earthquake epicenter. The present study include four earthquakes (M ≥ 6.0) (Nos. 4-7) earthquakes on the Palu-Koro fault, and three earthquakes (M≥6.5) (Nos. 1-3) on the Minahassa thrust, and one earthquake (M≥6.5) (No. 8) on the Poso fault (Figure 1). Since the earthquakes of M < 6.0 can only induce insignificant stress perturbance in a distance of about several tens of kilometers (Freed et al., 2007), they are excluded from this study.

The present study used a total of nine large earthquakes, including the 2018 Palu earthquake, as the earthquake sources for the calculations. The detailed earthquake source parameters are provided in Table S1 (see supporting information) and Figure 1.

3. ΔCFS partition and evolution on the Palu-Koro fault

The combined ΔCFS (co-seismic and post-seismic) distribution was calculated at a depth of 13 km (suggested hypocenter depth for the 2018 Palu earthquake) on the receiver faults with an identical focal mechanism (strike = 350°, dip = 67°, rake = -17°) to that of the 2018 Palu earthquake.

Figure 2(a) shows the cumulative ΔCFS map prior to 2018, which was induced by the three large earthquakes (Nos. 1~3) on the Minahassa thrust. Figure 3(a) details the induced ΔCFS distribution along the Palu-Koro fault. The ΔCFS exhibited an increase of approximately 50 kPa at the 2008 Palu earthquake hypocenter. This stress promotion is mainly contributed by the 1996 (M = 7.9) earthquake by comparing the Figures 3(a) and S2(a) to S3(c) (see supporting information).

Figure 2(b) shows the cumulative ΔCFS map prior to 2018, which was induced by the five large earthquakes (Nos. 4–8) on the Palu-Koro fault and the Poso fault. Figure 3(b) details the generated ΔCFS distribution along the Palu-Koro fault. The ΔCFS exhibited a minimal increase of only approximately 1 kPa at the 2008 Palu earthquake hypocenter by the combined effect of these events. However, the ΔCFS presented a significant decrease with the maximum values of -300 kPa and -290 kPa

to the north (zone P in Figure 3) and south (zone Q in Figure 3), respectively, of the 2018 Palu earthquake rupture (Figure 3(b)). These stress decreases were mainly contributed by the 1998 (M = 6.6) and 2012 (M = 6.3) earthquakes in these two zones (P and Q) on the Palu-Koro fault.

Figure 2(c) shows the cumulative ΔCFS map prior to 2018, which was induced by the eight large earthquakes (Nos. 1–8). Figure 3(c) details the induced Palu-Koro fault ΔCFS distribution. A combined ΔCFS of approximately 51 kPa was observed at the 2008 Palu earthquake hypocenter prior to 2018 induced by all these historical large earthquakes. The maximum ΔCFS drop was about -260 kPa and -280 kPa to the north (zone P in Figure 3) and south (zone Q in Figure 3), respectively, of the 2018 Palu earthquake rupture (Figure 2(c)).

Figure 2(d) shows the total ΔCFS map just after the 2018 Palu earthquake induced by the nine large earthquakes (Nos. 1–9). Figure 4 details the Palu-Koro fault ΔCFS distribution at the time intervals of 0, 20, 50, 100, 200, and 300 years after the 2018 Palu earthquake, assuming no further earthquake occur. Stress was released in most area between the epicenters of the 1998 (M6.6) and 2012 (M6.3) earthquakes on the Palu-Koro fault just after 2018 (Figure 2(d)). Two seismic gaps were left to the north (segment AB in Figure 4) and the south (segment CD in Figure 4) ends of the Palu-Koro fault. The ΔCFS in these gaps was increased on average by about 5 and 25 kPa just after the 2018 Palu earthquake (Figure 4). However, it will be increased to 19 and 45 kPa on average due to viscous relaxation in the ductile mantle over 100 years after the 2018 Palu earthquake (Figure 4).

The present study also investigate the sensitivity of the stress results relying on the model dependent parameters, such as, the dip and rake angles, frictional coefficient μ', and mantle viscosity η (see supporting information). By considering the uncertainty from all the model parameters, we found the ΔCFS promotion about 34-83 kPa at the hypocenter of the 2018 Palu earthquake prior to 2018. The maximum ΔCFS drop were about -242 to -390 kPa and -264 to -380 kPa to the north (zone P) and south ends (zone Q), respectively, of the 2018 Palu earthquake rupture. The average ΔCFS on the segments A'B' and CD will be promoted to approximately 7 ~ 21 kPa and approximately 37 ~ 56 kPa, respectively.

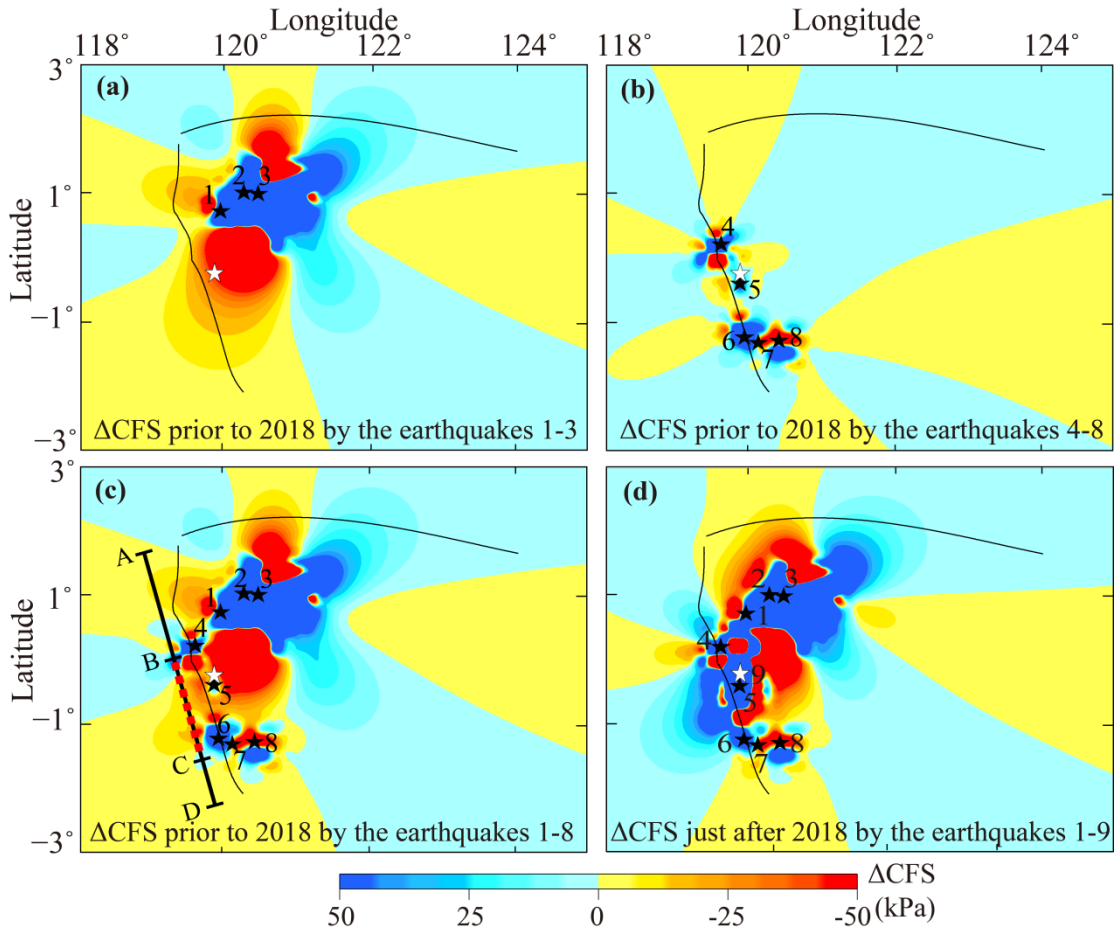

Figure 2: ΔCFS map at a depth of 13 km prior to and after 2018. (a) The cumulative ΔCFS map following the three earthquakes (Nos. 1–3) on the Minahassa thrust. (b) The cumulative ΔCFS map following the five earthquakes (Nos. 4–8) on the Palu-Koro fault and the Poso fault. (c) The cumulative ΔCFS map following eight earthquakes (Nos. 1–8) prior to the 2018 Palu earthquake. (d) The total ΔCFS map following the nine earthquakes (Nos. 1–9) just after the 2018 Palu earthquake. The epicenters of the earthquakes (Nos. 1–8) are marked with black stars. The epicenter of the 2018 Palu earthquake (No. 9) is marked by red star.

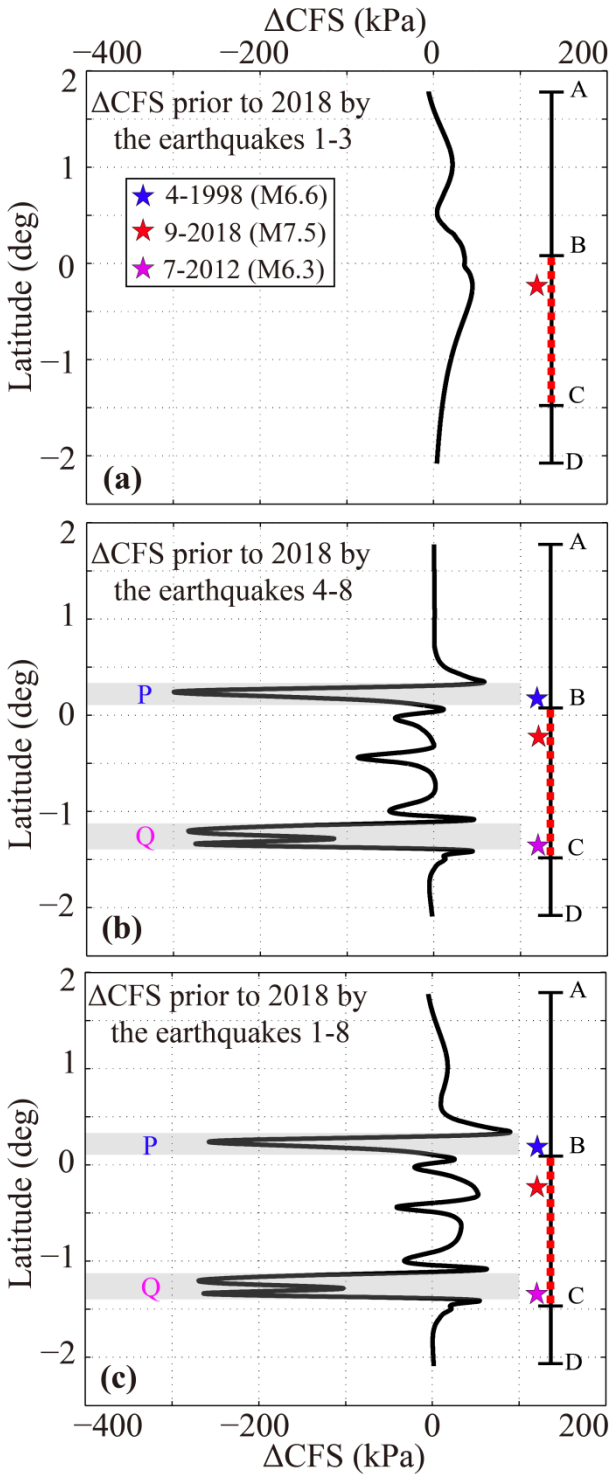

Figure 3: ΔCFS distribution along the Palu-Koro fault at a depth of 13 km prior to 2018. (a) The cumulative ΔCFS caused by the three earthquakes (Nos. 1–3) on the Minahassa thrust. (b) The cumulative ΔCFS caused by the five earthquakes (Nos. 4–8) on the Palu-Koro fault and the Poso fault. (c) The cumulative ΔCFS caused by the eight earthquakes (Nos. 1–8) prior to the 2018 Palu earthquake. The blue, pink, and red stars indicate the latitudes of the 1998 (M = 6.6), 2012 (M = 6.3), and 2018 Palu (Mw = 7.5) earthquakes, respectively. The red dash line indicates the 2018 Palu earthquake rupture on the Palu-Koro fault. The zones P and Q are marked grey.

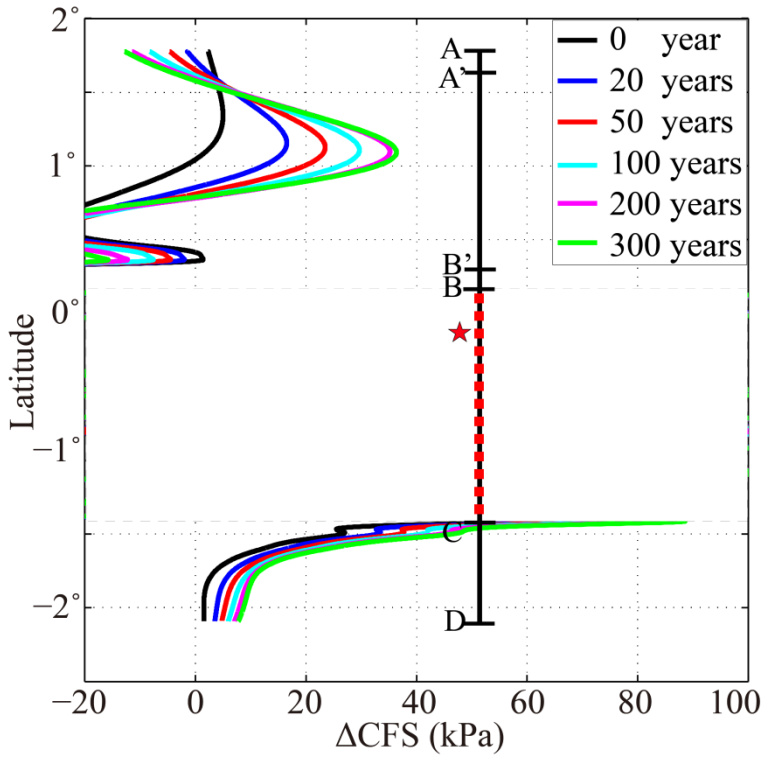

Figure 4: The total ΔCFS along the Palu-Koro fault at a depth of 13 km, which was induced by the nine earthquakes (Nos. 1-9) at the time intervals of 0, 20, 50, 100, 200, and 300 years after the 2018 Palu earthquake. The red star indicated the latitude of the epicenter of the 2008 Palu earthquake. The red dash line indicates the 2018 Palu earthquake rupture (segment BC) on the Palu-Koro fault.

4. Discussion

The stress field significantly affected the earthquake rupture process and seismic activities. The stress evolution in an earthquake circle in the Palu-Koro fault region was strongly influenced by several major factors, such as inter-seismic tectonic loading and stress perturbation that was induced by historic regional earthquakes. Temporally it is hard to simulate the inter-seismic tectonic loading in seismogenic depth of the Palu-Koro fault due to the unknown regional crustal structure through geodynamic modelling. However, the present study calculated the earthquake stress perturbation by calculating the Palu-Koro fault ΔCFS prior to the 2018 Palu earthquake, which was induced by eight large historical earthquakes surrounding the target area across several decades. We then identified a certain Palu-Koro fault location that had loaded or unloaded earthquake stress due to fault interaction prior to the 2018 Palu earthquake. As such, complex stress partition along the Palu-Koro fault strike was then observed (Figure 3(c)).

Our results show that the stress on the entire Palu-Koro fault prior to the 2018 Palu earthquake was promoted by the historical seismic activities of the Minahasaa thrust. The ΔCFS on the 2008 Palu earthquake hypocenter was increased about 51 kPa, which is mainly contributed by the 1996 (Mw = 7.9) earthquake on the Minahasaa thrust. In general, a positive ΔCFS resulted in an increase in the seismic activities in

the loaded stress regions. The observed value was much higher than the threshold (10 kPa) for triggering earthquakes (Reasenberg and Simpson,1992; King et al., 1994; Stein, 1999; Heidbach and Ben-Avraham, 2007). As such, the present study hypothesized that the 2018 Palu earthquake was triggered by historical seismic activities on the Minahassa thrust following earthquake triggering theory (Freed, 2005). The inter-seismic stress accumulation rate distribution along the entire Palu-Koro fault remains unclear. However, Vigny et al. (2002) calculated the maximum principal horizontal strain rate of about 311 and -291 nanostrain/a oriented 113°(±2°) using the geodetic data obtained on the Palu-Koro fault in the Palu basin. Based on this estimation, we could deduce a maximum principal stress rate of 3.11 and -2.91 kPa/a on the Palu-Koro fault assuming an elastic modulus of 1.0×10^{10} Pa. By integrating a roughly estimated tectonic loading Coulomb stress rate of approximately 1.0 kPa/a (approximately one third of the maximum principal stress rate), the promoted ΔCFS (51 kPa) was consistent with tectonic loading over approximately 51 years. This means the stress at the hypocenter of the 2018 Palu earthquake transferred by the historical earthquakes on the Minahassa thrust contributed to an equivalent stress loading of about 51 years of tectonic stress loading prior to the 2018 Palu earthquake. The stress results were significantly affected by model-dependent parameters, such as the Palu-Koro fault dip and rake angles, equivalent frictional coefficient, and mantle viscosity. A ΔCFS promotion of approximately 34 kPa to 83 kPa was observed at the 2018 Palu earthquake hypocenter prior to 2018 based on all the model parameter uncertainties, which still triggered the 2018 Palu earthquake following the earthquake triggering theory (Freed, 2005). These results reveal a significant control on the Palu-Koro fault seismic activity by the fault interaction between the Minahassa thrust and the Palu-Koro fault.

The Minahassa thrust and Palu-Koro fault interaction process is demonstrated by showing up the relationship between the inter-seismic crustal deformation due to tectonic loading and earthquake-induced crustal deformation in one map. Figure 5 shows the inter-seismic tectonic loading GPS velocity (Soquet et al., 2006) and the earthquake-induced (1996, Mw 7.9) crustal displacement (Gomez et al., 2000) near the Palu-Koro fault. The Palu-Koro fault tectonic loading stress was significantly affected by the shear, which was induced by the relative motion between the northwestward moving North Sula block and the southeastward moving Makassar block (Figure 5). Co-seismic displacements derived from GPS data (Vigny et al., 2002) and numerical modelling (Gomez et al., 2000) indicate that the 1996 (Mw = 7.9) earthquake led a northwestward motion of the North Sula block. This permanent earthquake-induced crustal displacement added a weight on the long-term Palu-Koro fault crustal motion (40 mm/yr) due to tectonic loading. It induced additional shear that superimposed the secular inter-seismic strain that resulted from the interaction between the North Sula block and the Makassar block (yellow arrows in Figure 5). Consequently, the transferred positive ΔCFS on the Palu-Koro fault triggered the 2018 Palu earthquake.

Our finding is congruent with the proposal of Vigny et al. (2002), which investigated the triggering effect on two 1998 (M = 6.6 and M = 6.3) Palu-Koro fault

earthquakes by a 1996 (Mw = 7.9) earthquake on the Minahassa thrust. Vigny et al. (2002) also indicated that Palu-Koro fault unclamping due to decreased normal stress may induce fluid migration into the fault plane of the Palu-Koro fault. The consequent increased pore pressure by the overpressured fluids in the fault plane might facilitate the Palu-Koro fault's rupture to promote the two 1998 earthquake. With respect to crustal deformation, the presented demonstration provides new perspectives on fault interaction between the Minahassa thrust and left-lateral strike-slip Palu-Koro fault. This finding is important for a comprehensive understanding the stress evolution and migration in a thrust and strike-slip fault system, globally. Two other examples are the southern San Andreas and nearby thrust and strike - slip faults (Lin and Stein, 2004) as well as the Longmen Shan (thrust) - Xianshui He (left-lateral strike-slip) fault system in eastern Tibet of Sichuan province, China (Liu et al., 2018). Our result might give an important clue to investigate the impact on the seismic activity on the Xianhui He fault by the 2008 Mw 7.9 Wenchuan earthquake on the Longmen Shan fault of eastern Tibet .

We also observed that the ΔCFS was decreased about -260 kPa to the north of the 2018 Palu earthquake rupture (zone P in Figure 3) caused by the 1998 (M = 6.6) on the Palu-Koro fault. Generally, a decrease in the negative ΔCFS seismic activities in the stress shadow regions. The presented approach investigated the effects of stress shadow of the 1857 Fort Tejon, 1897 Shillong Plateau, 1906 San Francisco, 1989 Loma Prieta, and 2008 Wenchuan earthquakes following a decrease in the ΔCFS (Simpson et al., 1988; Harris and Simpson, 1996; Harris, 1998; Freed and Lin, 2001; Freed, 2005; Mallman and Parsons, 2008; Gahalaut et al., 2011; Liu et al., 2018). A inter-seismic tectonic Coulomb loading stress rate of approximately 1.0 kPa/a was integrated, to which the ΔCFS release with the value -260 kPa was concordant with a tectonic loading of approximately 260 years. We proposed that the stress shadow in the zone P might act as a stress barrier preventing the earthquake rupture northward propagation and encourage its southward propagation.

It should be noted that we did not include the 1968 earthquake in our calculations of the ΔCFS due to a lack of reported focal mechanism and earthquake source parameters. The 1968 earthquake epicenter was located to the north of 2018 Palu earthquake. If this event was included in the calculation, we would expect a larger stress release in stress shadow zone to the north of the 2018 Palu earthquake rupture. The negative stress shadow stresses may have significantly limit the earthquake rupture's extending further to north. Vigny (2002) suggested that the two 1998 earthquakes enhanced earthquake inducement in the southern Palu-Koro fault region. According to our results, we suggested that 1998 (Mw 6.6) also had a great influence on the seismic activity on the north portion of the Palu-Koro fault by preventing the 2018 Palu earthquake rupture further propagating northward. The controlling effect of stress shadow on the faults rupture process is not unique for the 2018 Palu earthquake on the Palu-Koro fault. Previous studies suggested that the stress shadow in the LMSF southwest portion encouraged the unilateral northeastward rupture of the 2018 Mw 7.9 Wenchunan earthquake on the Longmen Shan fault (Liu et al., 2018). These findings may help characterize the earthquake rupture's propagation and termination

globally, such as the 2002 (Mw = 7.9) Denali fault earthquake's unilaterally eastward rupture (Eberhart-Phillips et al., 2003; Hreinsdóttir et al., 2013; Liu et al., 2018).

Our results also show that the ΔCFS was decreased about -280 kPa to the south end of the 2018 Palu earthquake rupture (zone Q in Figure 3) caused by the 2012 (M 6.3) earthquake on the Palu-Koro fault. A inter-seismic tectonic Coulomb loading stress rate of 1.0 kPa/a was integrated, to which the stress dropped to a value of -280 kPa that was concordant to a tectonic loading of approximately 280 years. Sensitivity test indicated that the ΔCFS drop ranged about -264 to -380 kPa in the zone Q. We believe that the stress drops with these values in the stress shadow zone Q are large enough to terminate the continuing southward propagation of the 2018 Palu earthquake rupture. This finding is congruent with those of Wang et al. (2019) who calculated the stress change by the 2005 (M = 6.2) and 2012 (M = 6.3) earthquakes, and confirmed the speculation of the stress drop stopping the 2018 earthquake rupture by Wei et al., (2018). The function of the stress shadow revealed by our study gave the reason for the termination of the 2018 Palu earthquake rupture.

After experiencing the five earthquakes (1998 (M = 6.6), 1998 (M = 6.2), 2005(M = 6.2), 2012 (M = 6.3), and 2018 (M = 7.5)) on the Palu-Koro fault during the past decades, two seismic gaps were left to the north and the south portions of the Palu-Koro fault. The average ΔCFS in these gaps was increased on average by about 5 and 25 kPa just after the 2018 Palu earthquake (Figure 4). However, it will be increased to 19 and 45 kPa due to ductile mantle viscous relaxation over 100 years after the 2018 Palu earthquake. Sensitivity test shows that the value of the ΔCFS on the segments A'B' and CD varies in the range of approximately 7 to 21 kPa and approximately 37 to 56 kPa (see supporting information), respectively, which is higher than the stress trigger threshold of 10 kPa. We believe that the promoted stress will be increasing the potential of the seismic hazards in the gaps in some degree. If the whole segments A'B' (130 km off-shore) and CD (120 km on-shore) rupture, which may have induced an sizable earthquake of $M \geq 7$, thus releasing accumulated strain at a rate close to 40 mm/yr over the past century [Stevens et al., 1999]. Close attention should be paid to the seismic and consequent tsunami hazards prevention in the central Sulawesi.

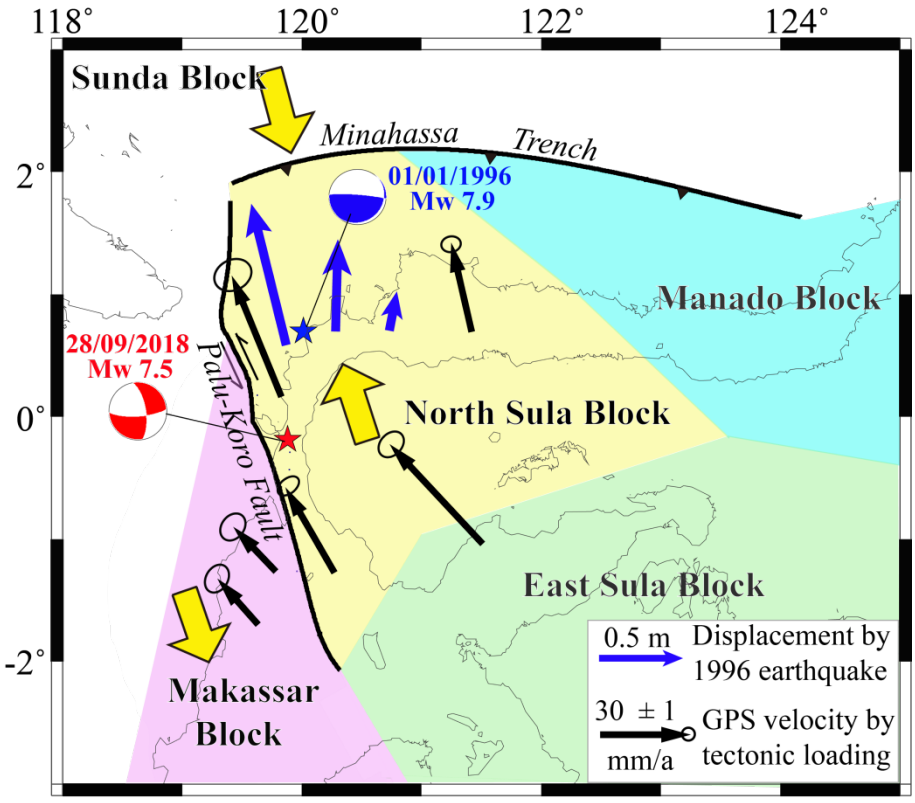

Figure 5: Schematic illustration of the interaction between the Palu-Koro fault and the Minahassa thrust by the relative motion of different regional blocks. Blue arrows indicates the crustal displacement induced by the 1996 earthquake (Mw7.9) on the Minahassa thrust (Gomez et al., 2000). The black arrow indicates the GPS velocity of the crust by tectonic loading (Socquet et al., 2006). The yellow arrow indicates the relative motion of the blocks constrained by different colors.

5. Conclusions

In order to investigate reasons for generating mechanism of the 2018 Palu earthquake and limiting the extent of the earthquake rupture, the present study calculated the Palu-Koro fault ΔCFS following the induction of historically large earthquakes along the Palu-Koro fault region with the past few decades. Future seismic hazards on the Palu-Koro fault was also investigated. We reached the following conclusions based on the stress partition and evolution process on the Palu-Koro fault:

(1) Fault interactions between the Minahassa thrust and the Palu-Koro fault triggered the 2018 Palu earthquake due to enhanced 2018 earthquake epicenter stress.

(2) The 2018 Palu earthquake rupture extent was significantly limited by the stress shadows that were induced by the historical Palu-Koro fault earthquakes. The stress shadow close to the north of the epicentre of the 2018 Palu earthquake acted as a stress barrier preventing the earthquake northward rupture, and encourage its southward propagation. However, the propagation was terminated by the stress shadow to the south of the earthquake rupture.

(3) Stress promotions in the two seismic gaps of the Palu-Koro fault in the north

and south portions of the Palu-Koro fault have increased the future seismic and tsunami hazards in the central Sulawesi.

Acknowledgements

This research was supported by the National Natural Science Foundation of China (No. 41974102), Shanghai Natural Science Foundation (No. 19ZR1459600), the Key Laboratory of Ocean and Marginal Sea Geology, Chinese Academy of Sciences (OMG2019-02), and the National Natural Science Foundation of China (No. U1839207, 41590865). The earthquake data used in this study is listed in Table in the main text. We are very grateful to Gregory Houseman for his constructive comments, which significantly improved the clarity and presentation of the results.

Reference:

Bao, H., Ampuero, J.P., Meng, L., Fielding, E.J., Liang, C., Milliner, C., Feng, T., Huang, H. Early and persistent supershear rupture of the 2018 Mw 7.5 Palu earthquake. Nat. Geosci. 2019, 12, 200–205.

Barka A. The 17 august 1999 Izmit earthquake. Science, 1999, 285: 1858-1859.

Barka A, Toda S, Stein R S. et al． Influence of the 17 August 1999 Izmit earthquake on seismic hazards in Istanbul． The 1999 Izmit and Duzce Earthquakes: Preliminary Results, Istanbul, 2000.

Beaudouin, T. 1998. Tectonique active et sismotectoni que du syste`me de failles de´crochantes de Sulawesi Central. The`se de Doctorat, Universita´ Paris Sud.

Bellier, O., Sébrier, M., Beaudouin, T., Villeneuve, M., Braucher, R., Bourles, D., ... & Pratomo, I. (2001). High slip rate for a low seismicity along the Palu‐Koro active fault in central Sulawesi (Indonesia). Terra Nova, 13(6), 463-470.

Katili, J.A. 1970. Additional evidence of transcurrent faulting in Sumatra and Sulawesi. Bandung National Institute of Geology and Mining Bulletin, 3, 15 28.

Cevikbilen, S., & Taymaz, T. (2019). Source Characteristics of the 28 September 2018 M w 7.5 Palu-Sulawesi, Indonesia (SE Asia) Earthquake Based on Inversion of Teleseismic Bodywaves. Pure and Applied Geophysics, 1-16.

Eberhart-Phillips, D., Haeussler, P. J., Freymueller, J. T., Frankel, A. D., Rubin, C. M., Craw, P., …& Dawson, T. E. (2003). The 2002 Denali fault earthquake, Alaska: A large magnitude, slip-partitioned event. Science, 300(5622), 1113-1118.

Fang, J., Xu, C., Wen, Y., Wang, S., Xu, G., Zhao, Y., & Yi, L. The 2018 Mw 7.5 Palu Earthquake: A Supershear Rupture Event Constrained by InSAR and Broadband Regional Seismograms. Remote Sensing, 2019, 11(11), 1330.

Freed, A.M.,&Lin, J. (2001).Delayed triggering of the 1999 Hector Mine earthquake by viscoelastic stress transfer. Nature, 411(6834), 180-183.

Freed, A.M. (2005).Earthquake triggering by static, dynamic, and postseismic stress transfer. Annual Review of Earth and Planetary Sciences, 33(335-367.

Freed, A.M., Ali, S.T.,&Bürgmann, R. (2007).Evolution of stress in Southern California for the past 200 years from co-seismic, postseismic and inter-seismic stress changes. Geophysical Journal International, 169(3),

1164-1179.

Gahalaut, V., Rajput, S.,&Kundu, B. (2011).Low seismicity in the Bhutan Himalaya and the stress shadow of the 1897 Shillong Plateau earthquake. Physics of the Earth and Planetary Interiors, 186(3), 97-102.

Gomez, J. M., Madariaga, R., Walpersdorf, A., & Chalard, E. (2000). The 1996 earthquakes in Sulawesi, Indonesia. Bulletin of the Seismological Society of America, 90(3), 739-751.

Hreinsdóttir, S., Freymueller, J. T., Fletcher, H. J., Larsen, C. F., & Bürgmann, R. (2003). Co-seismic slip distribution of the 2002 Mw7. 9 Denali fault earthquake, Alaska, determined from GPS measurements. Geophysical Research Letters, 30(13).

Harris, R. A. Forecasts of the 1989 Loma Prieta, California, earthquake. Bulletin of the Seismological Society of America, 1998, 88(4), 898-916.

Harris, R.A.,&Simpson, R.W. (1996).In the shadow of 1857-the effect of the Great Ft. Tejon Earthquake on subsequent earthquakes in southern California. Geophysical Research Letters, 23(3), 229-232.

Hall, R. 1996. Reconstructing Cenozoic SE Asia. In: Hall, R. & Blundell, D.J. (eds) Tectonic Evolution of SE Asia. Geological Society, London, Special Pub lications, 106, 153 184, https://doi.org/10.1144/GSL.SP.1996.106.01.11.

Jamelot, A., Gailler, A., Heinrich, P., Vallage, A., & Champenois, J. Tsunami simulations of the Sulawesi M w 7.5 event: Comparison of seismic sources issued from a tsunami warning context versus post-event finite source. Pure and Applied Geophysics, 2019, 176(8), 3351-3376

Hreinsdóttir, S., Freymueller, J. T., Fletcher, H. J., Larsen, C. F., & Bürgmann, R. (2003). Co-seismic slip distribution of the 2002 Mw7. 9 Denali fault earthquake, Alaska, determined from GPS measurements. Geophysical Research Letters, 30(13).

Heidbach, O.,&Ben-Avraham, Z. (2007).Stress evolution and seismic hazard of the Dead Sea fault system. Earth and Planetary Science Letters, 257(1), 299-312.

Jaumé, S.C.,&Sykes, L.R. (1996).Evolution of moderate seismicity in the San Francisco Bay region, 1850 to 1993: Seismicity changes related to the occurrence of large and great earthquakes. Journal of Geophysical Research: Solid Earth, 101(B1), 765-789.

King, G. C., Stein, R. S., & Lin, J. (1994). Static stress changes and the triggering of earthquakes. Bulletin of the Seismological Society of America, 84(3), 935-953.

Li, Z., Zhou, B. Influence of fault steps on rupture termination of strike-slip earthquake faults. J. Seismol. 2017, 22, 487–498.

Lin J, Stein R S. Stress triggering in thrust and subduction earthquakes and stress interaction between the southern San Andreas and thrust and strike-slip faults. J Geophys Res, 2004, 109(10): 1029-1047.

Liu, C., Dong, P.Y., Shi, Y.L. Stress change from the 2015 Mw 7.8 Gorkhar earthquake and increased hazard in the southern Tibetan Plateau. Physics of the Earth and Planetary Interiors, 2017, 267: 1-8.

Liu, C., Dong, P., Zhu, B., & Shi, Y. Stress shadow on the southwest portion of the Longmen Shan fault impacted the 2008 Wenchuan earthquake rupture. Journal of Geophysical Research: Solid Earth, 2018, 123(11), 9963-9981.

Mccaffrey R, Silver E A, Raitt R W. Crustal structure of the Molucca Sea collision zone, Indonesia[M]//The tectonic and geologic evolution of Southeast Asian seas and islands. Washington, DC: AGU, 1980, 23: 161-177.

Mallman, E.P.,&Parsons, T. (2008).A global search for stress shadows. Journal of Geophysical Research: Solid Earth, 113(B12), 1-16.

McCloskey, J., Nalbant, S.S.,&Steacy, S. (2005).Indonesian earthquake: Earthquake risk from co-seismic stress. Nature, 434(7031), 291-291.

Nostro, C., Cocco, M.,&Belardinelli, M.E. (1997).Static stress changes in extensional regimes: an application to southern Apennines (Italy). Bulletin of the Seismological Society of America, 87(1), 234-248.

Gahalaut V K , Rajput S, Kundu B. Low seismicity in the Bhutan Himalaya and the stress shadow of the 1897 Shillong Plateau earthquake. Physics of the Earth and Planetary Interiors, 2011,186(3), pp.97-102

Parsons, T., Ji, C.,&Kirby, E. (2008).Stress changes from the 2008 Wenchuan earthquake and increased hazard in the Sichuan basin. Nature, 454(7203), 509-510.

Panet, I., Pollitz, F., Mikhailov, V., Diament, M., Banerjee, P., & Grijalva, K. (2010). Upper mantle rheology from GRACE and GPS postseismic deformation after the 2004 Sumatra‐Andaman earthquake. Geochemistry, Geophysics, Geosystems, 11(6).

Pollitz F F, Bürgmann R, Banerjee P. Post-seismic relaxation following the great 2004 Sumatra-Andaman earthquake on a compressible self-gravitating Earth[J]. Geophysical Journal International, 2006, 167(1): 397-420.

Pollitz F, Banerjee P, Grijalva K, et al. Effect of 3-D viscoelastic structure on post-seismic relaxation from the 2004 M= 9.2 Sumatra earthquake[J]. Geophysical Journal International, 2008, 173(1): 189-204.

Simpson, R., Schulz, S., Dietz, L.,&Burford, R. (1988).The response of creeping parts of the San Andreas fault to earthquakes on nearby faults: two examples. Pure and Applied Geophysics, 126(2-4), 665-685.

Socquet, A., Simons, W., Vigny, C., McCaffrey, R., Subarya, C., Sarsito, D., ... & Spakman, W. (2006). Microblock rotations and fault coupling in SE Asia triple junction (Sulawesi, Indonesia) from GPS and earthquake slip vector data. Journal of Geophysical Research: Solid Earth, 111(B8).

Socquet, A.; Hollingsworth, J.; Pathier, E.; Bouchon, M. Evidence of supershear during the 2018 magnitude7.5 Palu earthquake from space geodesy. Nat. Geosci. 2019, 12, 192–199.

Song, X.; Zhang, Y.; Shan, X.; Liu, Y.; Gong,W.; Qu, C. Geodetic observations of the 2018 Mw 7.5 Sulawesi earthquake and its implications for the kinematics of the Palu fault. Geophys. Res. Lett. 2019, 46, 4212–4220.

Stein, R.S., King, G.C.,&Lin, J. (1994).Stress triggering of the 1994 M= 6.7

Northridge, California, earthquake by its predecessors. Science, 265(5177), 1432-1432.

Stevens, C., McCaffrey, R., Bock, Y., Genrich, J., Subarya, C., Puntodewo, S. S. O., & Vigny, C. (1999). Rapid rotations about a vertical axis in a collisional setting revealed by the Palu fault, Sulawesi, Indonesia. Geophysical Research Letters, 26(17), 2677-2680.

Ulrich, T., Vater, S., Madden, E. H., Behrens, J., van Dinther, Y., van Zelst, I., ... & Gabriel, A. A. Coupled, Physics-based Modeling Reveals Earthquake Displacements are Critical to the 2018 Palu, Sulawesi Tsunami. Pure and Applied Geophysics, 2019, 1-41.

Vigny, C., Perfettini, H., Walpersdorf, A., Lemoine, A., Simons, W., van Loon, D., & Bock, Y. (2002). Migration of seismicity and earthquake interactions monitored by GPS in SE Asia triple junction: Sulawesi, Indonesia. Journal of Geophysical Research: Solid Earth, 107(B10).

Wang R, Kuempel H J. Poroelasticity: efficient modeling of strongly coupled, slow deformation processes in a multi-layered half-space. Geophysics, 2003, 68(2): 705-717.

Wang R, Lorenzo F, Roth F. Computation of deformation induced by earthquakes in a multi-layered elastic crust-FORTRAN pro-grams EDGRN/EDCMP. Comput Geosci-UK, 2003, 29: 195-20.

Wang, S., Xu, C., Xu, W., Yin, Z., Wen, Y., & Jiang, G. (2018). The 2017 M w 6.6 Poso Earthquake: Implications for Extrusion Tectonics in Central Sulawesi. Seismological Research Letters, 90(2A), 649-658.

Wang, Y., Feng, W., Chen, K., & Samsonov, S. Source Characteristics of the 28 September 2018 Mw 7.4 Palu, Indonesia, Earthquake Derived from the Advanced Land Observation Satellite 2 Data. Remote Sensing, 2019, 11(17), 1999.

Watkinson, I. M., & Hall, R. (2017). Fault systems of the eastern Indonesian triple junction: evaluation of Quaternary activity and implications for seismic hazards. Geological Society, London, Special Publications, 441(1), 71-120.

Wei, S.; Feng, G.; Zeng, H.; Martin, S.; Shi, Q.; Muzli, M.; Wang, T.; Lindsey, E.; Triyono, R.; Hubbard, J.; et al. The 2018 Mw 7.5 Palu Earthquake, a Gradually Accelerating Super-Shear Rupture Stopped by Stress Shadows in a Complex Fault System; AGU Fall Meeting Abstracts: Washington, DC, USA, 2018.

Wells, D.L.,&Coppersmith, K.J. (1994).New empirical relationships among magnitude, rupture length, rupture width, rupture area, and surface displacement. Bulletin of the Seismological Society of America, 84(4), 974-1002.

Walpersdorf, A., Vigny, C., Subarya, C., & Manurung, P. (1998). Monitoring of the Palu‐Koro Fault (Sulawesi) by GPS. Geophysical Research Letters, 25(13), 2313-2316.

Supporting information

S1. Historical Earthquakes

The four large historical earthquakes on the Palu-Koro fault are the May 21st, 1998 (M = 6.6), October 10th, 1998 (M = 6.0), January 23rd, 2005 (M = 6.3), and August 18th, 2012 (M = 6.2) earthquakes. The focal mechanism of the two 1998 earthquakes were provided by Vigny et al. (2002) using a body-wave inversion. However, the surface ruptures of these earthquakes are unknown since they originated off-shore (Watkinson and Hall, 2016). The focal mechanism of the 2005 earthquakes and the 2012 earthquakes are available from the United States Geological Survey (USGS) centroid moment tensor (CMT) catalogue.

The three 1996 earthquakes (Mw = 7.9, Mw = 6.6, and Mw = 7.0) occurred between January and July 1996 along the Minahassa subduction zone in northwestern Sulawesi. The focal mechanisms of these earthquakes were provided by Gomez et al. (2000) through a body-wave inversion. In his study the Mw 7.9 earthquake fault slip model was also investigated through co-seismic deformation modelling using global positioning system (GPS) data, and was chosen as earthquake source in this study.

The May 29th, 2017 earthquake (Mw = 6.6) occurred on the Poso fault in the Tokorondo complex (Wang et al., 2018). The source parameters of the main earthquake were estimated by Wang et al. (2018) using interferometric synthetic aperture radar (InSAR) data inversion, which was used as earthquake source in this study.

Previous studies have revealed the fault rupture process of the 2018 Palu Mw 7.5 earthquake using seismic wave, GPS, and InSAR data inversions (Bao et al., 2019; Fang et al., 2019; Socquet et al., 2019; Song et al., 2019; Ulrich et al., 2019; Wang et al., 2019a, 2019b; Cevikbilen et al., 2019; USGS). The present study used the fault slip model developed by Song (2019) as it exhibited a geometrical simplicity and comparable slip distribution as compared to the other models (Bao et al., 2019; Socquet et al., 2019; Song et al., 2019; Wang et al., 2019).

The mechanisms of the other six earthquakes are available from the U.S. Geological Survey (USGS) cen-troid moment tensor (CMT) catalogue. Rectangular planar patches with uniform slips define the early earthquake fault planes, since well-constrained co-seismic dislocation distributions are not available. The down-dip length of the earthquake planes on the Palu-Koro fault and Minahassa thrust refers to the fault planes of the 2018 Palu earthquake and Jan 1st 1996 earthquake, respectively (Gomez et al., 2000; Fang et al., 2019). The along-strike length of the earthquake planes and slip magnitude were inferred by estimating the rupture areas based on the empirical scaling laws and relationships defined by Wells and Coppersmith (1994). The detailed earthquake source parameters are provided in Table S1.

Table S1: Model parameters for the historical earthquakes on and around the Palu-Koro fault.

No.	Date	Magnitude	Location		Strike/Dip/Rake	Length (km)	Width (km)	Slip (m)	Ref.
			Latitude	Longitude					
0	14/08/1968	7.2	0.157°	119.80°	*	*	*	*	A
1	01/01/1996	7.9	0.73°	119.93°	53°/7°/68°	90	60	1.8	B
2	16/07/1996	6.6	1.02°	120.25°	63°/14°/ 71°	20	19	0.6	A
3	22/07/1996	7.0	1.00°	120.45°	57°/ 14°/ 63°	40	18	1.1	A
4	21/05/1998	6.6	0.21°	119.58°	195°/ 74 °/20°	21	20	0.62	C
5	10/10/1998	6.0	-0.40°	119.84°	250°/ 94°/ 96°	15	20	0.22	C
6	23/01/2005	6.2	-1.239°	119.9°	321°/61°/ -59°	18	20	0.26	A
7	18/08/2012	6.3	-1.326°	120.092°	339°/83°/ -5°	20	20	0.31	A
8	29/05/2017	6.6	-1.292	120.4	104°/44°/ -95°	16	11	1.2	D
9	28/09/2018	7.5	-0.256	119.846	350°/67°/ -17°	#	#	#	E

Note: The earthquake parameters were extracted from the following sources: (A) USGS earthquake catalogue; (B) Gomez et al., 2000; (C) Vigny et al., 2002; (D) Wang et al., 2018; (E) Song et al., 2019; and # refers to E for finite fault parameters and * refers to unavailable earthquake parameters. Length and width means along-strike and down-dip length, respectively.

S2. Methodology

The Coulomb stress change (Harris, 1998) defines the ΔCFS as follows:

$\Delta CFS = \Delta\tau_s + \mu' \Delta\sigma_n$ (1),

where $\Delta\tau_s$ and $\Delta\sigma_n$ define variations in the shear and normal stresses, respectively; and μ' defines the coefficient of equivalent friction, which ranges between 0.2 and 0.8.

The lithospheric structure and rheological structure in the vicinity of the Palu-Koro fault is not documented. The present study developed the lithospheric model parameters based on the Crust-2 model and the lithospheric rheological structure of the surrounding region, specifically the Malucca sea collision zone (Mccaffrey and Silver, 1980) and the Sumatra region (Vigny et al., 2002; Pollitz et al., 2006, 2008; Panet et al., 2010). The designed model presented a 30-km thick crust with an overlying 70-km thick lithospheric mantle. The parameter summary of the two-layer lithospheric model is presented in Table S2. The lithospheric mantle has a viscosity of 1.0×10^{19} Pa·s, which is higher than the estimated viscosity of the Palu-Koro fault region mantle (1.0×10^{18} Pa·s) as suggested by Vigny et al. (2002).

However, it is consistent with the estimates of the viscosity of lithospheric mantle in Sumatra region using post-seismic deformation simulation (Pollitz et al., 2006, 2008; Panet et al, 2010). We altered the viscosity value within a realistic range to evaluate the impact of viscosity on the calculated ΔCFS. We chose a low value of 0.4 for the equivalent friction coefficient, μ', given the requirements for a relatively smooth fault plane to generate the 2018 Palu earthquake super-shear rupture process (Bao et al., 2019). This value was subsequently modified to assess its effect on the calculated ΔCFS.

Table S2: Lithospheric model layer parameters, where H is the thickness, G is the elastic shear modulus, η is the viscosity, CR is the crust, and LM is the lithospheric mantle.

Layers	H (km)	ρ (kg/m$^{3)}$	G (Pa)	η (Pa.s)
CR	30	2700	8.5×10^{10}	1.0×10^{23}
LM	70	3200	1.7×10^{11}	1.0×10^{19}

Previous studies reported the 2018 Palu Mw 7.5 earthquake fault parameters using seismic wave, GPS, and INSAR data inversions (Bao et al., 2019; Fang et al., 2019; Socquet et al., 2019; Song et al., 2019; Ulrich et al., 2019; Wang et al., 2019a, 2019b; Cevikbilen et al., 2019; USGS). The employed fault-plane segments, fault geometries, and slip distributions differed due to inversion differences in the modelling techniques and data sets. Regardless of the differences in detail in some local area on the fault, the different solutions have much in common. Firstly, the rupture initiated from the hypocenter and propagated northward by approximately 20 km to 30 km. Conversely, the rupture stroke southward for approximately 130 km to 140 km, (Fang et al., 2019; Socquet et al., 2019; Song et al., 2019). Secondly, previous studies well-confined the Palu-Koro fault strike with the variation of 352° and 356°. Thirdly, the dominant strike-slip fault motion took place on a plane dipping at approximately 67° to 85° along strike and with the rake varying about -17° to -30°. The present study changed the values of the dip and rake angles in several end-member cases to evaluate their impact on the calculated ΔCFS.

The present study employed the PSGRN/PSCMP code (Wang et al., 2003, 2006) to estimate the ΔCFS from the layered lithospheric model dislocation sources. The ΔCFS was calculated based on the co-seismic and post-seismic stress contributions prior to 2018 from historical earthquakes (listed in Table S1) that took place in the vicinity over the past decades. In order to examine the ΔCFS evolution after 2018, we also simulated the co-seismic and post-seismic stress induced by the 2018 Palu earthquake.

S3. Stress result

S3.1. ΔCFS by historical earthquake

Figures S1(a)–S1(c) present the ΔCFS map induced by the three large

earthquakes (Nos. 1–3) on the Minahassa thrust prior to 2018. Figures S2(a) to S2(c) show the ΔCFS distribution details along the Palu-Koro fault as a result of each event. The 1996 earthquake (M 7.9) promoted ΔCFS almost on the entire Palu-Koro fault with the maximum value of 50 kPa near the 2008 Palu earthquake hypocenter (Figures S1(a) and S2(a)). The two other 1996 earthquakes (M = 6.6 and M = 7.0) enhanced the Palu-Koro fault ΔCFS with the exception of a short segment (Figures S2(b) and S2(c)). However, a relatively small ΔCFS value of approximately 0.1 kPa to 0.2 kPa was measured due to their limited magnitudes (M = 6.6 and M = 7.0) and the long distances (>300 km) between their epicenters and the Palu-Koro fault (Figures 1(b), 1(c), 2(b) and 2(c)).

Figures S1(d) to S1(h) present the ΔCFS map that was individually induced by five large earthquakes (Nos. 4–8) on the Palu-Koro fault and the Poso fault prior to 2018. Figure S2(d) to S2(h) show the resulting ΔCFS distribution details along the Palu-Koro fault. All these events enhanced ΔCFS at the 2018 Palu earthquake hypocenter (Figures S1(d) to S1(h)), except for the 1998 (M = 6.6) earthquakes, which decreased the ΔCFS by about -5 kPa (Figure S2(d)). However, the promoted ΔCFS was quite small and ranged between 0.1 kPa and 5 kPa at the 2018 earthquake hypocenter. The results also indicate that the 1998 (M = 6.6) and 2012 (M = 6.3) earthquakes decreased the ΔCFS with the maximum stress drop of about -300 kPa and -280 kPa to the north and south ends of the 2018 Palu earthquake rupture, respectively (Figure S2(d) and S2(g)).

Figure S1(i) presents the co-seismic ΔCFS map as induced by the 2018 Palu Mw 7.5 earthquake, and Figure S2(i) details the ΔCFS distribution along the Palu-Koro fault as a result of this event. Stress was released in most areas of the rupture zone following this event. The maximum ΔCFS drop was about -4 MPa. However, it was promoted in the south portion of the Palu-Koro fault, which was not activated by the 2018 Palu earthquake (Figure S1(i)).

Figures S3(a) to S3(f) show the map shows the spatial variation of the modeled ΔCFS at the time intervals of 0, 20, 50, 100, 200, and 300 years after the 2018 Palu earthquake, assuming no further earthquake occur.

Table S3 summarizes the ΔCFS evolution with time at different location on the Palu-Koro fault.

Table S3: The ΔCFS evolution with time at different location on the Palu-Koro fault. 'Hypo' means the 2018 Palu earthquake hypocenter. The locations of different zone and segment on the Palu-Koro fault are indicated in Figure 5. It summarizes the maximum ΔCFS drop in the narrow zones P and Q, and the average ΔCFS promotion in segments A'B' and CD. The ΔCFS is reported in kPa.

	Prior to 2018			0 year after 2018		100 years after 2018	
	Hypo	P	Q	A'B'	CD	A'B'	CD
ΔCFS	51	-260	-280	5	25	19	45

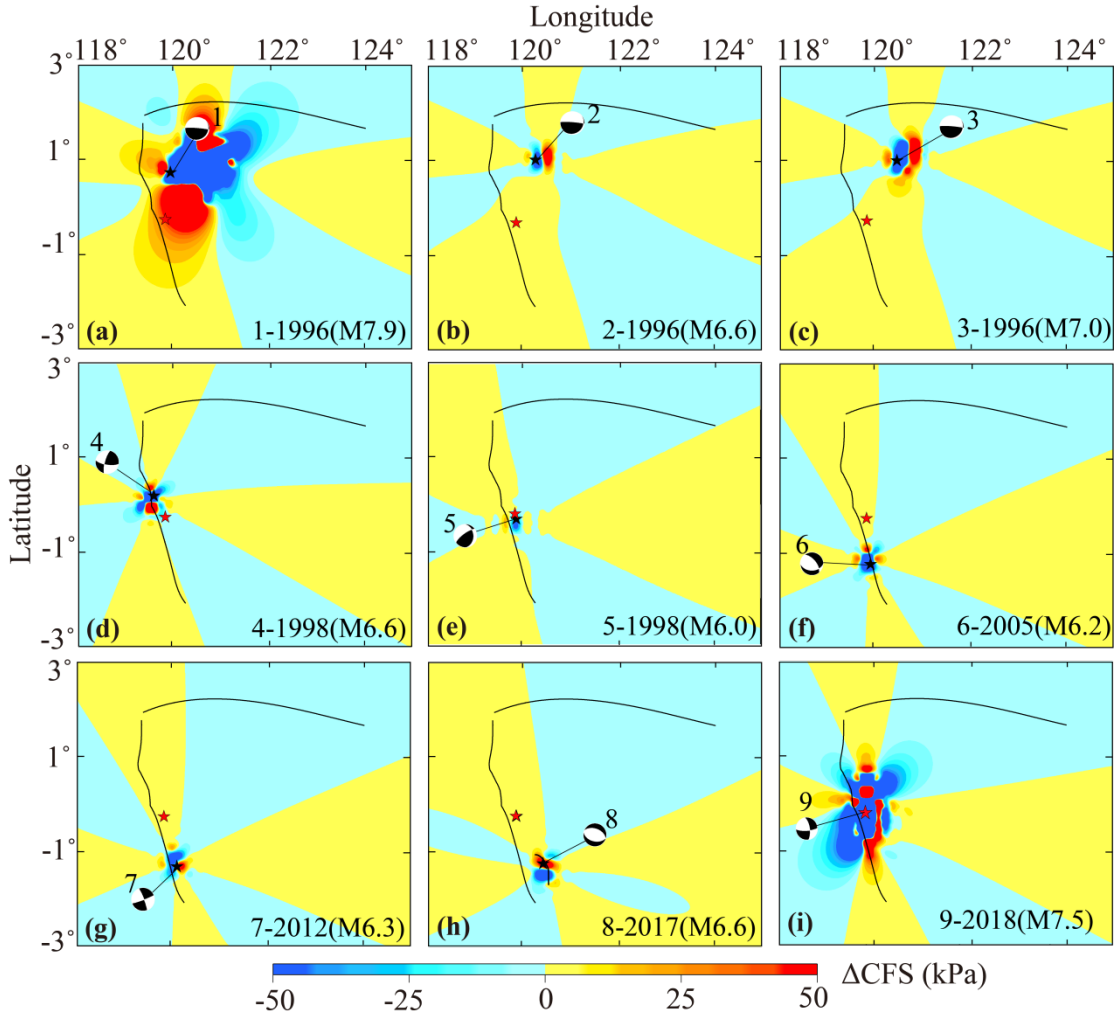

Figure S1: ΔCFS Map at a depth of 13 km prior to and in 2018. The ΔCFS Map prior to 2018 was a result of: (a) the 1996 earthquake (Mw = 7.9); (b) the 1996 earthquake (Mw = 6.6); (c) the 1996 earthquake (Mw = 7.0); (d) the 1998 earthquake (M = 6.6); (e) the 1998 earthquake (M = 6.0); (f) the 2005 earthquake (M = 6.2); (g) the 2012 earthquake (M = 6.3); and (h) the 2017 earthquake (M = 6.6). (i) The 2018 earthquake-induced co-seismic ΔCFS (Mw = 7.5). The faults are represented by black lines. The epicenters of the earthquakes Nos. 1–8 were marked with black stars. The epicenter of the 2018 Palu earthquake (No. 9) was marked with red star.

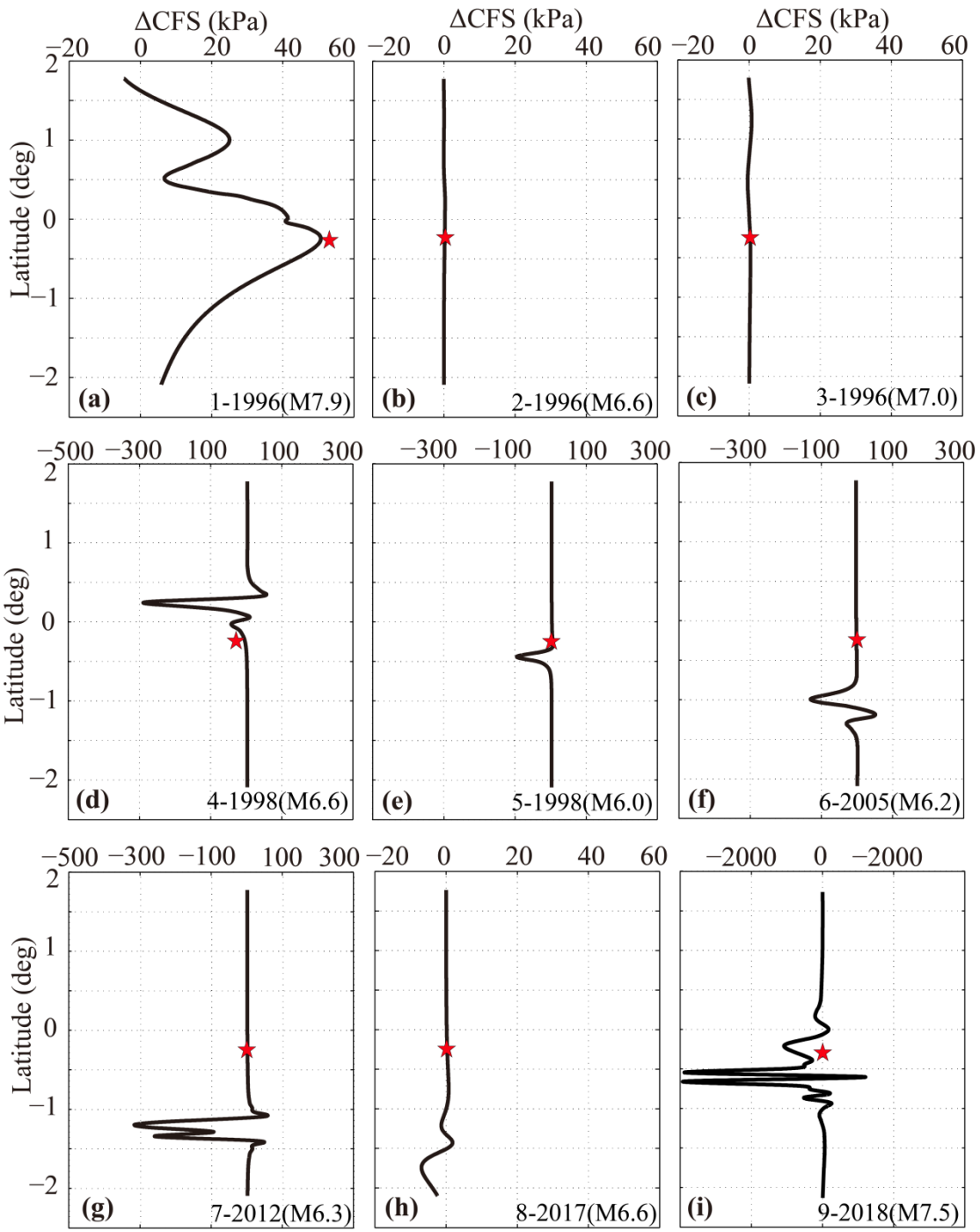

Figure S2: ΔCFS along the Palu-Koro fault at a depth of 13 km prior to and in 2018. ΔCFS prior to 2018 was a result of: (a) the 1996 earthquake (Mw = 7.9); (b) the 1996 earthquake (Mw = 6.6); (c) the 1996 earthquake (Mw = 7.0); (d) the 1998 earthquake (M = 6.6); (e) the 1998 earthquake (M = 6.0); (f) the 2005 earthquake (M = 6.2); (g) the 2012 earthquake (M = 6.3); and (h) the 2017 earthquake (M = 6.6). (i) The 2018 Palu earthquake-induced co-seismic ΔCFS (Mw = 7.5). The red star defines the 2018 Palu earthquake latitude.

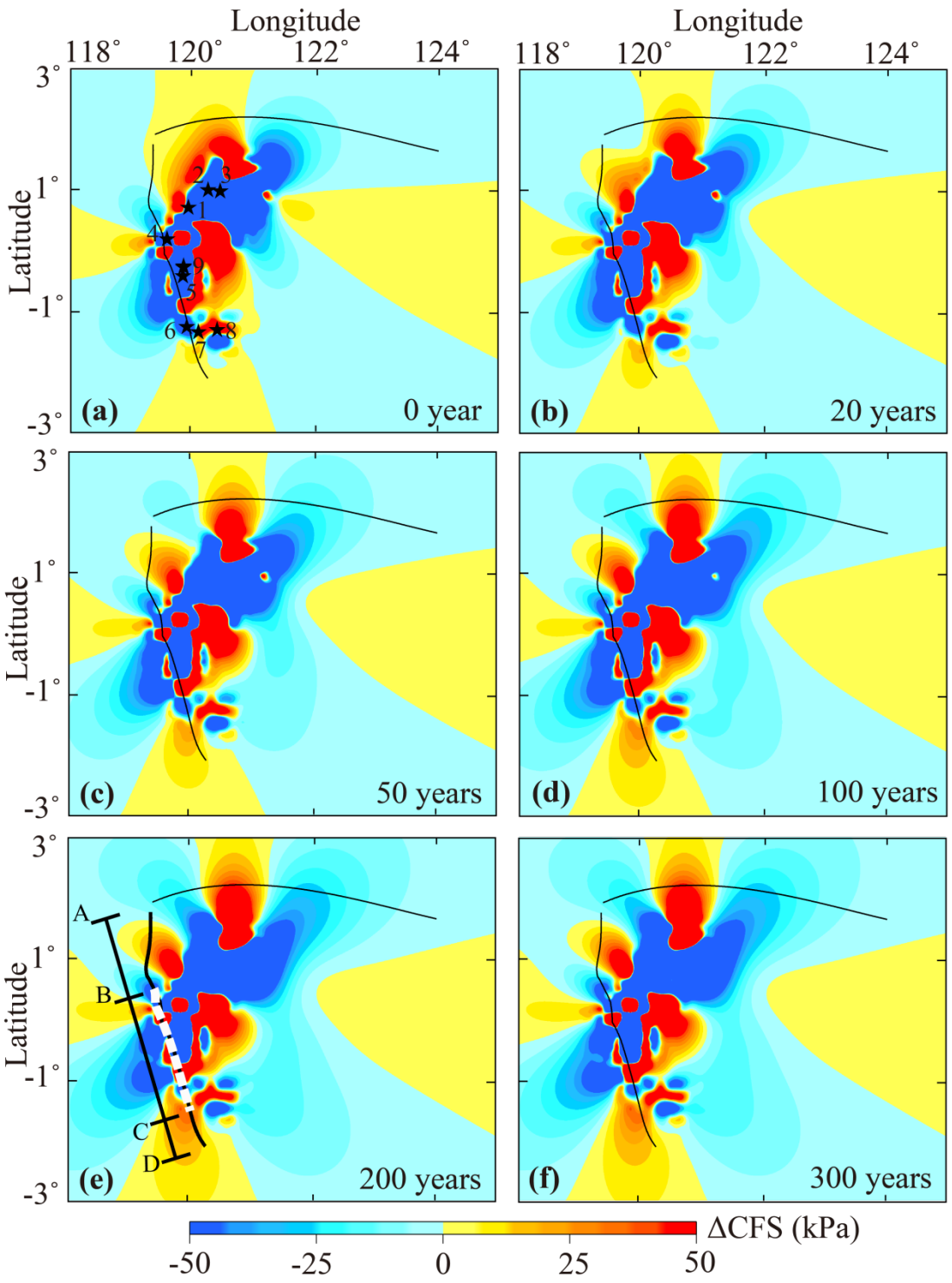

Figure S3: Map of the total ΔCFS at a depth of 13 km, which was induced by the nine earthquakes at the time intervals of (a) 0, (b) 20, (c) 50, (d) 100, (e) 200, and (f) 300 years after the 2018 Palu earthquake. The epicenters of the earthquakes are marked with black stars in (a). The white dash line indicates the 2018 Palu earthquake rupture on the Palu-Koro fault.

S3.2. Sensitivity of the stress results

The present study varied only one model parameter to investigate the sensitivity

of the stress results for each case, such that all other parameters remained constant based on the above model setting (reference model Case 0) for the following calculation. The following model parameters were applied to the reference model: strike = 350°, dip = 67°, rake = -17°, μ' = 0.4, η = 1.0×10^{18} Pa·s. The dip and rake angles, frictional coefficient μ', and mantle viscosity η, were varied.

4.2.1. Influence of the dip angle

Previous fault slip model reported that dip angle of the Palu-Koro fault varied from 67° to 85° with distance (Bao et al., 2019; Fang et al., 2019; Socquet et al., 2019; Song et al., 2019; Ulrich et al., 2019; Wang et al., 2019; Cevikbilen et al., 2019; USGS). Based on these observations, the present study calculated the Palu-Koro fault ΔCFS using the dip angle 85° in another case.

Figure S4 (a) shows the ΔCFS along the Palu-Koro fault with different dip angle prior to 2018 by the eight earthquakes (Nos. 1-8). Figure S5(a) shows the ΔCFS along the Palu-Koro fault with different dip angle over 100 years after the 2018 Palu earthquake by the nine earthquakes (Nos. 1-9). Table S4 summarizes the detailed ΔCFS of different locations on the Palu-Koro fault. A comparison of the stress results indicate that this variation in the Palu-Koro fault dip angle minimally affected the stress of the 2018 Palu earthquake hypocenter (Figure S4(a)) and the segments A'B' and CD (Figure S5(a)). The ΔCFS presented a minimal decrease of approximately 7 kPa at the 2018 Palu earthquake hypocenter following an increase in the dip angle from 67° to 85°, whereas an average ΔCFS increase of approximately 3 kPa to 4 kPa was observed on the A'B' and CD segments (Table S4). However, it significantly influenced the stress to the north and south ends of the 2018 Palu earthquake rupture (Figure S5(a)). Varying the dip angle from 67° to 85° increased the maximum ΔCFS drop from -260 kPa to -320 kPa and from -280 kPa to -344 kPa in the zones P and Q, correspondingly (Table S4).

4.2.2. Influence of the rake

Different fault slip models suggested a rake angle difference between -17° and -30° (Bao et al., 2019; Fang et al., 2019; Socquet et al., 2019; Song et al., 2019; Ulrich et al., 2019; Wang et al., 2019a, 2019b; Cevikbilen et al., 2019; USGS). We then used the dip angles of -30°in the other case for the ΔCFS calculation.

Figures S4(b) shows the ΔCFS along the Palu-Koro fault with different rake angle prior to 2018 by the eight earthquakes (Nos. 1-8). Figures S5(b) shows the ΔCFS along the Palu-Koro fault with different rake angle over 100 years after the 2018 Palu earthquake by the nine earthquakes (Nos. 1-9). Table S5 summarizes the detailed ΔCFS of different location on the Palu-Koro fault. Results indicate that the rake angle had a minor impact on the stress of the entire Palu-Koro fault (Figures S4(b) and S5(b)). It only decreased the ΔCFS of 5 kPa at the 2018 Palu earthquake hypocetner by increasing the dip angle from 67° to 85°. The generated variation in the ΔCFS in zones P and Q was only approximately 2 kPa to 4 kPa. It nearly had no impact on the ΔCFS of the segments A'B' and CD (Table S5).

4.2.3. Influence of the μ'

The present study selected an appropriate equivalent frictional coefficient, μ', and connected this to the normal stress component in the ΔCFS calculations. In general, ΔCFS calculations varied the μ' value between 0.2 and 0.8. The present study applied values of 0.2, 0.6, and 0.8 in the three additional cases to test the influence of μ' on the ΔCFS.

Figure S4 (c) shows the ΔCFS along the Palu-Koro fault with different μ' prior to 2018 by the eight earthquakes (Nos. 1-8). Figures S5 (c) shows the ΔCFS along the Palu-Koro fault with different μ' over 100 years after the 2018 Palu earthquake by the the nine earthquakes (Nos. 1-9). Table S6 summarizes the detailed ΔCFS of different location on the Palu-Koro fault. Results indicate that varying μ' have a significant impact on the stress of the 2018 Palu earthquake hypocenter and zones P and Q (Figure S4(c)). An increase in μ' from 0.2 to 0.8 changed the ΔCFS from 45 kPa to 83 kPa at the 2018 Palu earthquake hypocenter (Table S6). It increased the maximum ΔCFS drop from -242 kPa to -350 kPa and from -264 kPa to -380 kPa in the zones P and Q, respectively (Table S6). However, it had minor impact on the segments A'B' and CD, on which the average ΔCFS was only increased by 5~7 kPa (Table S6).

4.2.4. Influence of the viscosity

At present, the mantle viscosity in the Palu-Koro fault area is poorly known. As such, the present study calculated the ΔCFS against two viscosity configurations to test the impact of viscosity on ΔCFS. Previous calculations (Case 0) applied a mantle viscosityof 1.0×10^{19} Pa·s (η_0). We increased the viscosities by 10-fold in Case 1 (η_1) and decreased the viscosities by 10-fold in Case 2 (η_2).

Figure S4(d) shows the ΔCFS along the Palu-Koro fault with different viscosity prior to 2018 by the eight earthquakes (Nos. 1-8). Figures S5 (d) shows the ΔCFS along the Palu-Koro fault with different viscosity over 100 years after the 2018 Palu earthquake by the nine earthquakes (Nos. 1-9). Table S7 summarizes the detailed ΔCFS of different location on the Palu-Koro fault. Results indicated that the viscosity had a relatively large impact on the ΔCFS (Figures S4(d) and S5(d)). Enlarging the viscosity 100-fold from 1.0×10^{18} to 1.0×10^{20} Pa·s promoted the ΔCFS from 34 kPa to 64 kPa at the hypocenter of the 2018 Palu earthquake. Consequently, the maximum ΔCFS drop decreased from -390 kPa to -250 kPa in zone P, while it increased from -272 kPa to -290 kPa in the zone Q. It also decreased the average ΔCFS from 10 to 7 kPa and from 56 to 37 kPa on the segments A'B' and CD, respectively (Table S7).

Thus, by considering the uncertainty from all the model parameters, we found the ΔCFS promotion about 34-83 kPa at the hypocenter of the 2018 Palu earthquake prior to 2018. The maximum ΔCFS drop were about -242 to -390 kPa and -264 to -380 kPa to the north (zone P) and south ends (zone Q), respectively, of the 2018 Palu earthquake rupture. The average ΔCFS on the segments A'B' and CD will be promoted to approximately 7 ~ 21 kPa and approximately 37 ~ 56 kPa, respectively.

Table S4: The ΔCFS evolution with time at different location on the Palu-Koro fault with different dip angle. 'Hypo' means the hypocenter of the 2018 Palu earthquake. The locations of different zone and segment on the Palu-Koro fault are indicated in Figure S5. It summarizes the maximum ΔCFS drop in the zones P and Q, and the average ΔCFS promotion in segments A'B' and CD. The ΔCFS is reported in kPa.

Dip	Prior to 2018			100 years after 2018	
	Hypo	P	Q	A'B'	CD
67°	51	-260	-280	19	45
85°	44	-320	-344	21	49

Table S5: The ΔCFS evolution with time at different location on the Palu-Koro fault with different rake angle. 'Hypo' means the hypocenter of the 2018 Palu earthquake. The locations of different zone and segment on the Palu-Koro fault are indicated in Figure S5. It summarizes the maximum ΔCFS drop in the zones P and Q, and the average ΔCFS promotion in segments A'B' and CD. The ΔCFS is reported in kPa.

Rake	Prior to 2018			100 years after 2018	
	Hypo	P	Q	A'B'	CD
-17°	51	-260	-280	19	45
-30°	46	-262	-276	19.5	46

Table S6: The ΔCFS evolution with time at different location on the Palu-Koro fault with different μ'. 'Hypo' means the hypocenter of the 2018 Palu earthquake. The locations of different zone and segment on the Palu-Koro fault are indicated in Figure S5. It summarizes the maximum ΔCFS drop in the zones P and Q, and the average ΔCFS promotion in segments A'B' and CD. The ΔCFS is reported in kPa.

	Prior to 2018			100 years after 2018	
μ'	Hypo	P	Q	A'B'	CD
0.2	45	-242	-264	16	43
0.4	51	-260	-280	19	45
0.6	78	-304	-328	20	47
0.8	83	-350	-380	21	50

Table S7: The ΔCFS evolution with time at different location on the Palu-Koro fault with different viscosity of the mantle. 'Hypo' means the hypocenter of the 2018 Palu earthquake. The locations of different zone and segment on the Palu-Koro fault were indicated in Figure S5. It summarizes the maximum ΔCFS drop in the zones P and Q, and the average ΔCFS increase in segments A'B' and CD. The ΔCFS is reported in kPa.

	Prior to 2018			100 years after 2018	
Viscosity	Hypo	P	Q	A'B'	CD
η_1	64	-250	-290	7	37
η_0	51	-260	-280	19	45
η_2	34	-390	-272	10	56

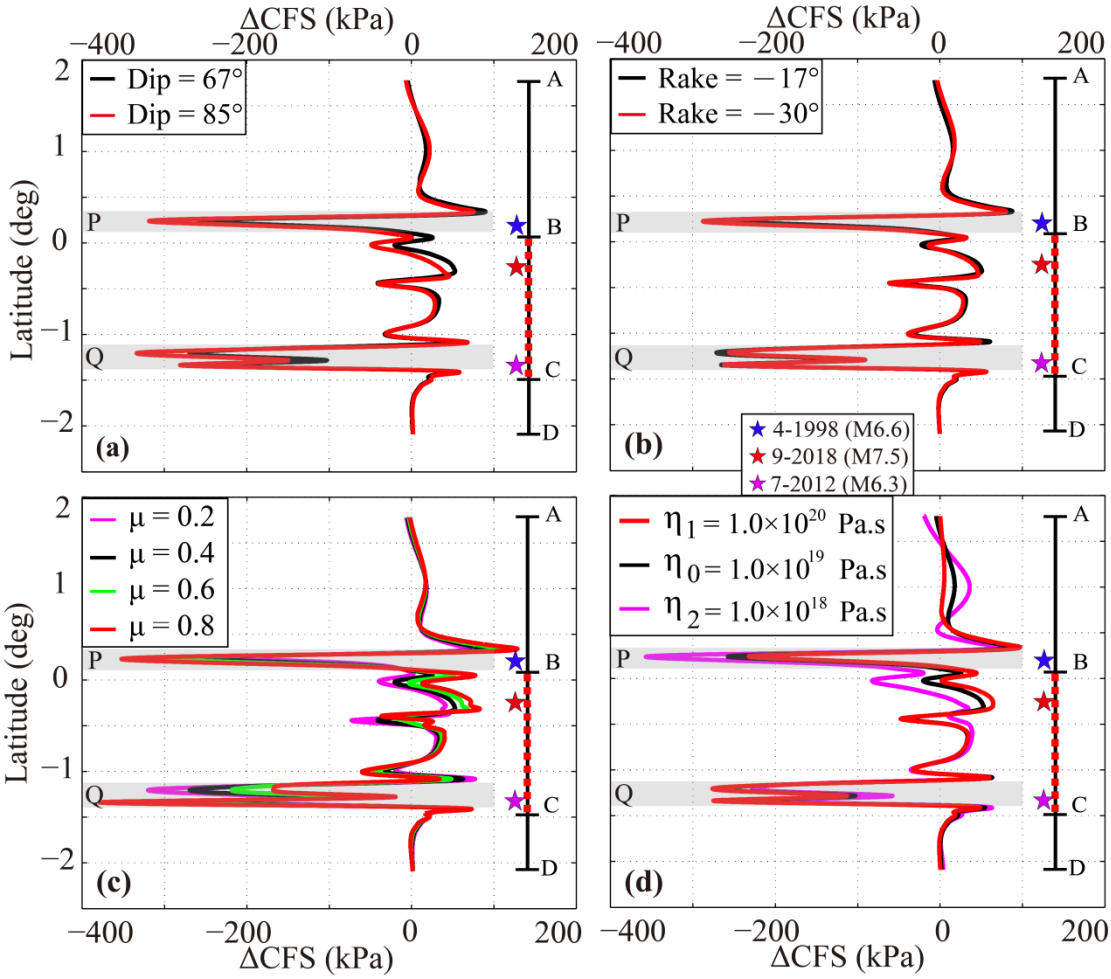

Figure S4: The ΔCFS along the Palu-Koro fault at a depth of 13 km prior to the 2018 Palu earthquake, which was induced by the eight earthquakes (Nos. 1–8) for various model parameters (a) dip angle, (b) rake angle, (c) μ', and (d) viscosity. The blue, red, and pink stars indicate the latitudes of the 1998 (M = 6.6), the 2018 Palu (Mw = 7.5), and the 2012 (M = 6.3) earthquakes, correspondingly. The red dashed line indicates the 2018 Palu earthquake rupture (BC) on the Palu-Koro fault (AD). The zones P and Q are painted grey.

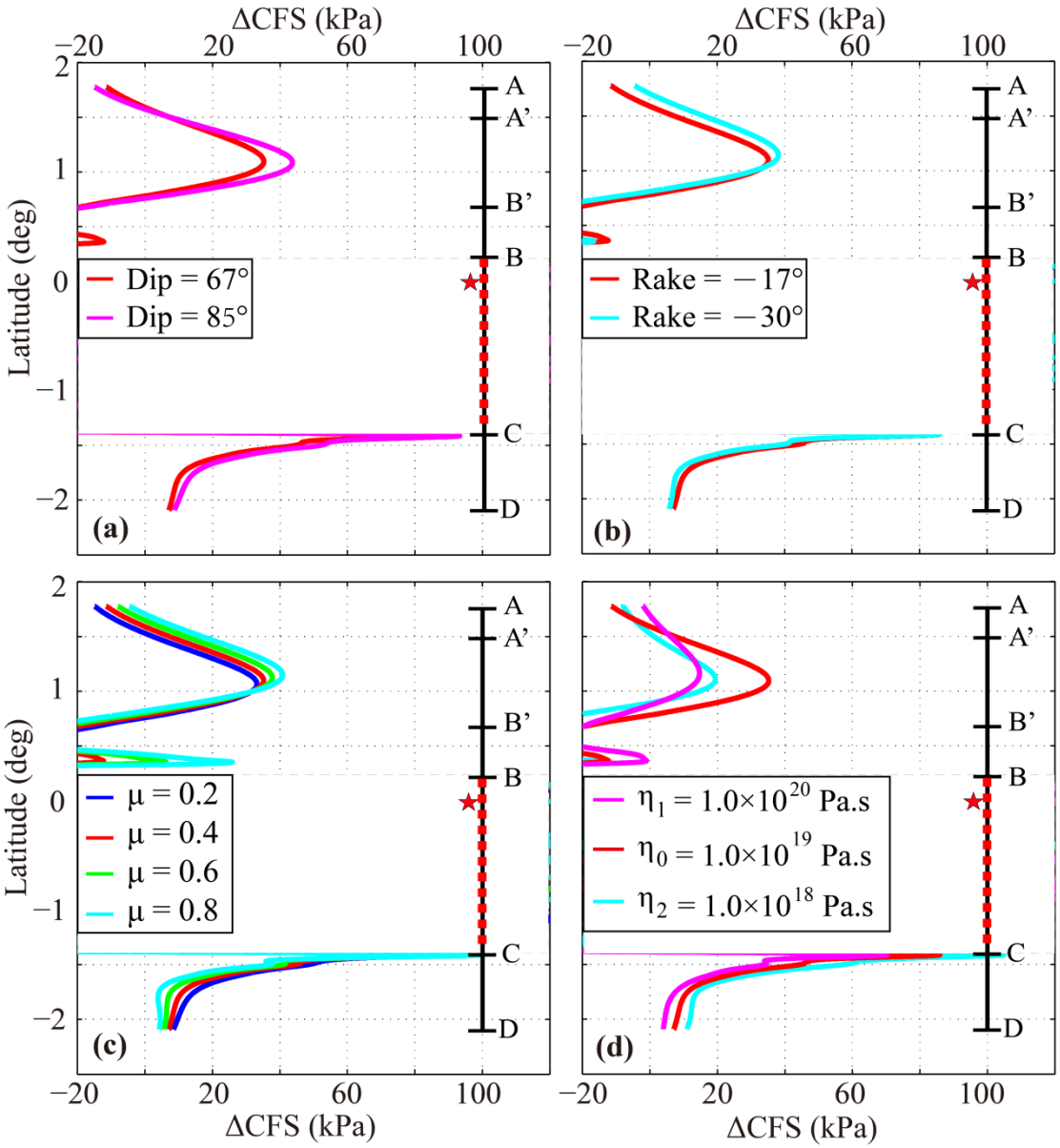

Figure S5: The ΔCFS along the Palu-Koro fault at the depth of 13 km over 100 years after the 2018 Palu earthquake, which was produced by the nine earthquakes for various model parameters (a) dip angle, (b) rake angle, (c) μ', and (d) viscosity. The red star defines the latitudes of the 2008 Palu earthquake epicenters. The red dashed line defines the 2018 Palu earthquake rupture on the Palu-Koro fault.